XPS and XAFS Pt $L_{2,3}$-Edge Studies of Dispersed Metallic Pt and PtSn Clusters on SiO_2 Obtained by Organometallic Synthesis: Structural and Electronic Characteristics

José M. Ramallo-López,[†] Gerardo F. Santori,[‡,§] Lisandro Giovanetti,[†] Mónica L. Casella,[‡] Osmar A. Ferretti,*[,‡,§] and Félix G. Requejo[†,||]

Instituto de Física de La Plata (IFLP) (CONICET) and Departamento de Física, Facultad de Ciencias Exactas, Universidad Nacional de La Plata, 49 y 115 (1900) La Plata, Argentina, Centro de Investigación y Desarrollo en Ciencias Aplicadas "Dr. Jorge Ronco" (CINDECA), Facultad de Ciencias Exactas, and Departamento de Ingeniería Química, Facultad de Ingeniería, Universidad Nacional de La Plata, 47 No. 257 − C.C. 59 − (1900) La Plata, Argentina, and Materials Science Division, Lawrence Berkeley National Laboratory, Berkeley, California 94706

Received: May 8, 2003; In Final Form: July 23, 2003

In this work, well-defined silica-supported Pt and PtSn catalysts were prepared by surface organometallic reactions and were characterized by EXAFS-XANES at the Pt $L_{2,3}$ edge and XPS of the Pt 4f and Sn 3d levels. These catalysts were tested in the catalytic hydrogenation of cinnamaldehyde in the liquid phase. XPS results showed that in PtSn−OM* (not having butyl groups anchored on the surface), tin was present as Sn(0) adatoms "decorating" the metallic surface, isolating Pt atoms; in the PtSn−OM catalyst (Bu groups remain grafted on the surface), tin was found in the form of Sn(0) and Sn(II, IV) in similar proportions. EXAFS experiments do not provide evidence of the existence of PtSn alloys in any of these systems. In the bimetallic PtSn−BM systems, it was possible to observe by XPS that tin was found in the form of Sn(0) and Sn(II, IV). EXAFS experiments, in this case, allowed us to demonstrate the existence of a PtSn alloy diluting metallic Pt atoms. In tin-modified systems, when a fraction of ionic tin is present, the activation of the C═O group of the cinnamaldehyde is favored, increasing the selectivity to UOL. An increase in the number of Pt 5d holes measured by Pt-$L_{2,3}$ XANES could be indicating as a d → s, p rehybridization process in the PtSn 3D small nanoclusters present in PtSn−BM catalysts.

Introduction

Bimetallic catalysts based on Pt modified by a second metal (Sn, Pb, Ge) have been gaining importance, from their classical utilization in the reforming process of naphthas up to their use in reactions concerning environmental and fine chemistry.[1,2]

Obtaining well-defined active phases in their nature and composition leads to systems with better global catalytic properties, and for this reason the development and comprehension of controlled-preparation techniques of solid catalysts have maintained permanent interest. One of these techniques is surface organometallic chemistry on metals (SOMC/M), which allows us to obtain bimetallic and organobimetallic catalysts with very good activity, selectivity, and stability in hydrogenation and dehydrogenation reactions and is useful in obtaining synthesis gas.[3−5]

The state of the base monometallic catalyst, Pt/SiO_2, in the case of the present work plays a fundamental role in the preparation of the bimetallic system. Thus, taking into account the superficial character of the reaction between the organometallic ($SnBu_4$) and Pt/SiO_2, it is important to find this last one highly dispersed, so its characterization is more difficult from conventional methods.

The knowledge of the structure of small bimetallic particles will contribute to the understanding and improvement of their catalytic activity. In addition to aspects traditionally analyzed in monometallic catalysts (structure and electronic properties of small supported metal clusters), the characterization of bimetallic catalysts includes the nature elucidation of the interaction between the metals at low dimensionalities. This has already been discussed in detail by Rodríguez and Goodman on model surfaces,[6] but systems with lower dimensionalities are still an open field. Besides, in the case of PtSn catalysts studied in this work, an adequate explanation of its functioning is closely related to the Sn oxidation state. For instance, some results found in the literature[7] indicate that, for $PtSn/SiO_2$ catalysts having particle sizes between 2 and 20 nm, Pt and Sn atoms in the same particle do not necessarily present a uniform distribution. A newly developed atomic-resolution in situ TEM[8] could be helpful in elucidating the location and oxidation state of the promoter under reaction conditions, so it would be possible to explain its influence upon the catalytic activity. Another technique that has been very useful in the study of highly dispersive bimetallic systems is energy-dispersive X-ray spectrometry, which gives detailed information about particle sizes and their composition.[9,10] X-ray photoelectron spectroscopy (XPS) is another adequate technique for carrying out this type of characterization.[11]

XAFS spectroscopy is nowadays one of the most powerful methods of local-order characterization in highly dispersed metal catalysts.[12,13] This method is especially useful for investigating the environment of very small metal particles, which are very difficult to study by other techniques. In many cases, information can be obtained in situ during the different steps of preparation such as calcination, reduction, and even during catalytic reaction,

* Corresponding author. E-mail: ferretti@quimica.unlp.edu.ar.
[†] Instituto de Física de La Plata (IFLP) (CONICET) and Departamento de Física, Universidad Nacional de La Plata.
[‡] Centro de Investigación y Desarrollo en Ciencias Aplicadas "Dr. Jorge Ronco" (CINDECA), Universidad Nacional de La Plata.
[§] Departamento de Ingeniería Química, Universidad Nacional de La Plata.
[||] Lawrence Berkeley National Laboratory.

10.1021/jp030579y CCC: $25.00
Published on Web 09/20/2003

when the catalyst becomes inaccessible to traditional surface-analysis techniques. Usually, it is very difficult to perform structural investigations in systems with concentrations of modifying components below 1%. It has been shown in the literature that the XAFS methods might be used successfully with very small concentrations of modifying components and could provide information about the local geometry and electronic properties of the atoms in very dilute systems.[14] Extended X-ray absorption fine structure (EXAFS) spectroscopy gives information about the surroundings of the absorber atom. In the particular case of Pt, the study of the L_3 absorption edge measuring the transmission of X-rays provides information about the kind, number, and distance of neighbors around Pt atoms. XANES (X-ray absorption near-edge spectroscopy) gives information about the electronic state of the absorbing element. For platinum atoms, the study of L_2 and L_3 edges gives information on the density of unoccupied 5d states, measuring the transition of core electrons to this band. Using the method described by Mansour et al., it is possible to determine the variation in the density of unoccupied d states in a sample containing Pt with respect to Pt foil.[15]

In this work, we present EXAFS-XANES at the Pt $L_{2,3}$ edge and XPS of Pt 4f- and Sn 3d-level studies performed on Pt and PtSn catalysts supported on SiO_2, with the aim of gaining knowledge about the localization and state of the species of the metallic phase for a better comprehension of the catalytic behavior. Also, the modifications in the Pt electronic structure and the effects they cause were studied. For this purpose, a test reaction of applied interest was selected, such as the hydrogenation of cinnamaldehyde.

Experimental Section

Catalyst Preparation. A Degussa silica (Aerosil 200, 200 $m^2\ g^{-1}$) was used as support. The silica was suspended in NH_4OH(aq) under stirring prior to the addition of the $[Pt(NH_3)_4]^{2+}$ solution, having a concentration so as to obtain 1% w/w Pt exchanged on the silica. The solid was kept under stirring for 24 h at 298 K, and then the suspension was separated by filtration under vacuum. The solid was repeatedly washed, dried at 378 K, calcined in air at 773 K, and reduced in flowing H_2 at the same temperature, leading to the monometallic Pt/SiO_2 catalyst.

The tin-modified catalysts preparation consisted of the reaction of a solution of $SnBu_4$ in a paraffinic solvent (*n*-heptane when the preparation was conducted at 363 K and *n*-decane when the preparation temperature was at 423 K) with the reduced Pt/SiO_2 catalyst under flowing H_2. After 4 h of reaction, the liquid phase was separated, and the solid was repeatedly washed with *n*-heptane and subsequently dried in Ar at 363 K. The solids obtained after this procedure were identified as PtSn−OM (having butyl groups grafted to the surface) or PtSn−OM* (with no butyl groups grafted to the surface). The bimetallic phases (PtSn−BM) were obtained by elimination of the organic groups by activation of PtSn−OM catalysts in flowing H_2 at 773 K for 2 h. The variation in $SnBu_4$ concentration and the amount of hydrocarbons evolved during the preparation reaction were analyzed using a Varian 3400 CX gas chromatograph equipped with a flame ionization detector, employing a 10% OV-101 column ($^1/_8$ in. i.d., 0.5-m length) and a tricresyl phosphate column ($^1/_4$ in., 6-m length), respectively. Platinum and tin contents were determined by atomic absorption.

Hydrogen and CO Chemisorption. Hydrogen and CO chemisorption were measured in a static volumetric apparatus at room temperature. For each sample, a first adsorption isotherm was obtained for the sample previously reduced at 773 K for 4 h and then evacuated at the same temperature overnight. Afterward, the sample was submitted to an evacuation at room temperature for 2 h, and a second isotherm was measured in the same manner. The difference between the two isotherms extrapolated to zero pressure gave the amount of the irreversibly adsorbed hydrogen and CO (H/Pt and CO/Pt).

XPS Characterization. XPS data were obtained with an ESCA 750 Shimadzu spectrometer equipped with a hemispherical electron analyzer and a Mg Kα (1253.6 eV) X-ray source. Fresh samples were mounted onto a manipulator that allowed the transfer from the preparation chamber into the analysis chamber. PtSn−OM samples were dried, and PtSn−BM samples were reduced in situ at 673 K for 1 h. The binding energy (BE) of the C 1s peak at 284.6 eV was taken as an internal standard. The intensities were estimated by calculating the integral of each peak after subtracting the S-shaped background and fitting the experimental peak to a Lorentzian/Gaussian mix of variable proportion.

X-ray Absorption Spectroscopy. XAS cells are a glass ring, about 1-cm thick, with sealed Kapton windows used as sample holders. The samples were prepared as described below at the desired temperature in a glass reactor connected to the XAS cells. The powdered samples were transferred under Ar or H_2 to the XAS cells, which were then sealed. In the case of experiments performed in H_2 atmospheres, for Pt/SiO_2 and PtSn−BM catalysts, the reduction step was conducted in H_2 at 773 K, and PtSn−OM and PtSn−OM* catalysts were tested after preparation at 363 and 423 K, respectively. In the case of experiments performed in Ar atmospheres (Pt/SiO_2, PtSn−BM), catalysts were reduced in H_2 at 773 K and then treated in Ar at 773 K for 2 h.

X-ray absorption spectra were measured at the XAS beamline at the LNLS − National Synchrotron Light Laboratory, Campinas, Brazil. EXAFS and XANES spectra of the Pt L_3 edge (11.6 keV) and L_2 (13.3 keV) were recorded at room temperature using a Si(220) single channel-cut crystal monochromator in transmission mode and with two ion chambers as detectors.

EXAFS data were extracted from the measured absorption spectra by standard methods.[16,17] Raw data files were averaged, and the pre-edge region was approximated by a modified Victoreen curve. Normalization was completed by dividing by the height of the absorption edge, and the background was subtracted using cubic spline routines. The main contributions to the spectra were isolated by Fourier transformation of the final EXAFS functions. The analysis was performed on these Fourier-filtered data.

The absorption edge positions of a sample, defined as the major inflection point in the edge, are a function of the oxidation state of the element and shift to a higher energy as the oxidation state of the absorbing element becomes higher than zero.[18]

At the Pt L_3 edge, the allowed bound-state to bound-state transition from $2p_{3/2}$ to vacant d states of the absorbing atom gives rise to a resonance peak (white line) above the edge due to vacancies in the 5d level of Pt. The line shape of the resonance contains information on the type of final state involved in the transition. Lytle et al.[19] have shown that increases in the resonance peak intensity with respect to pure element absorbers correlate with the ionicity estimated from the number of d electrons removed from the element by the formation of chemical bonds. Lytle[20] has also shown that the L_3 resonance peak areas for the third-row transition metals increased from Au to Ta, which is also the sequence for increased electron vacancies in the d band. Meitzner et al.[21] have found similar

results for Re, Os, Ir, Pt, and Au. They also observed that the resonance for the metal in a highly dispersed state was only slightly more intense than it was for the bulk form of the metal, indicating a small electron deficiency of the highly dispersed form relative to the bulk. To quantify the differences in white-line intensity between the catalyst and platinum foil, a variation of the method described by Mansour et al.[15] was used.[22] After subtracting the platinum foil data of the catalyst data, the resulting curves were numerically integrated between −10 and +14 eV for both the L_2 (ΔA_2) and L_3 (ΔA_3) edges using

$$f_d = \frac{\Delta A_3 \sigma_3 + 1.11 \Delta A_2 \sigma_2}{A_{3r} \sigma_3 + 1.11 A_{2r} \sigma_2} \quad (1)$$

The fractional change in the total number of unfilled states in the d band of the sample compared to the number in the platinum foil (f_d) was calculated. The areas are normalized[23] by multiplying by the X-ray absorption cross section at the edge jump (σ). Values of 117.1 and 54.2 $cm^2\ g^{-1}$ were used for the absorption cross section at the platinum L_3 and L_2 edges,[24] respectively. When the number of unfilled d states in the reference material (h_{Tr}) is known, the number of unfilled d states in the sample (h_{Ts}) can be calculated from

$$h_{Ts} = (1 + f_d)\, h_{Tr} \quad (2)$$

Samples of Pt/SiO_2 and tin-modified platinum catalysts were measured to determine the Pt surroundings. This enables us to know if its neighborhood was modified by the incorporation of tin so that we can study the interaction between Pt and Sn in the tin-modified platinum catalysts to compare the number of unfilled d states in both samples and to correlate all of these properties with catalytic behavior.

EXAFS experiments were performed on Pt/SiO_2, PtSn−OM, and PtSn−BM samples to determine the nature, amount, and distance of first neighbors of Pt atoms.

Catalytic Test. The hydrogenation of cinnamaldehyde (Aldrich, 99+%) was carried out in a batch reactor, magnetically stirred at 800 rpm, introducing the reactant in a toluene solution (0.17 M). The temperature was kept at 313 K, and the pressure was kept at 0.1 MPa of H_2 during the experiment. The mass of catalyst was 0.5 g. Samples of the reaction products were analyzed using a Varian 3400 CX gas chromatograph equipped with a capillary column (30 m × 0.53 in. i.d., DB Wax bonded phase) and a FID detector.

Before being submitted to the hydrogenation test, Pt/SiO_2 and PtSn−BM catalysts were pretreated under flowing H_2, increasing the temperature from ambient to 773 K, and holding it for 2 h. PtSn−OM catalysts were prepared and tested in the same reactor to prevent any contact with the atmosphere.

Results

Preparation, H_2/CO Adsorption, and XPS Characterization of Tin-Modified Platinum Catalysts. The two-step anchoring process to prepare the PtSn−OM and PtSn−BM catalysts can be represented by the following reaction scheme:

$$363-423\ K:\ Pt/SiO_2 + y SnBu_4 + xy/2 H_2 \rightarrow Pt(SnBu_{4-x})_y/SiO_2 + xy BuH \quad (3)$$

$$423-773\ K:\ Pt(SnBu_{4-x})_y/SiO_2 + (4-x)y/2 H_2 \rightarrow PtSn_y/SiO_2 + (4-x)y BuH \quad (4)$$

TABLE 1: Composition and Denomination of the Studied Catalysts

entry	catalyst	Sn/Pt	stoichiometry
1	Pt/SiO_2		
2	PtSn−OM*[a]	0.06	$PtSn_{0.06}$
3	PtSn−OM*[a]	0.12	$PtSn_{0.12}$
4	PtSn−OM*[a]	0.20	$PtSn_{0.2}$
5	PtSn−OM[a]	0.30	$Pt(SnBu_{1.6})_{0.3}$
6	PtSn−OM[a]	0.40	$Pt(SnBu_{1.8})_{0.4}$
7	PtSn−OM[b]*	0.40	$PtSn_{0.4}$
8	PtSn−OM[b]	0.70	$Pt(SnBu_{1.6})_{0.7}$
9	PtSn−OM[b]	1.41	$Pt(SnBu_{2.7})_{1.4}$
10	PtSn−BM[a]	0.06	$PtSn_{0.06}$
11	PtSn−BM[a]	0.20	$PtSn_{0.2}$
12	PtSn−BM[a]	0.30	$PtSn_{0.3}$
13	PtSn−BM[a]	0.40	$PtSn_{0.4}$
14	PtSn−BM[b]	0.70	$PtSn_{0.7}$

[a] Prepared at 90 °C. [b] Prepared at 150 °C.

Blank experiments performed on silica via the above-described preparation procedure did not evidence either a variation in the concentration of tetra-*n*-butyltin between 298 and 423 K or a detectable concentration of tin in the solids.

The reaction between $SnBu_4$ and Pt/SiO_2 was followed by GC analysis, measuring the variation in $SnBu_4$ concentration in the impregnating solution and the total butane amount evolved per $SnBu_4$ reacted. Results obtained show that a temperature increase has a beneficial influence on both the $SnBu_4$ reacted with Pt/SiO_2 and the reaction rate (eq 3). In fact, at 363 K, it is possible to fix tin selectively onto platinum up to a Sn/Pt ratio of approximately 0.40, whereas it increases to 1.40 when the reaction temperature is 423 K. Table 1 shows results corresponding to different platinum/tin catalysts prepared. Data presented in Table 1 indicate that the cleavage of Sn−C bonds and the elimination of butyl groups as butane depend on the temperature. When reaction 3 is carried out at 363 K, there is complete removal of butyl groups provided that the Sn/Pt atomic ratio is kept under 0.2 (approximately 4BuH evolved per $SnBu_4$ reacted), whereas for the plateau (Sn/Pt ≅ 0.40) the amount of butane eliminated per fixed tin is near 2.2, leading to an organobimetallic-supported phase with a global stoichiometry of $Pt(SnBu_{1.8})_{0.4}/SiO_2$ (PtSn−OM-type phase). For higher temperatures, for example, 423 K, reaction 3 proceeds with a complete detachment of butyl groups as BuH, up to a Sn/Pt ratio close to 0.40 leading to a phase with a stoichiometry of $PtSn_{0.4}/SiO_2$, whereas for Sn/Pt ≅ 1.40 an evolution of approximately 1.3 butane per fixed tin is observed and the organobimetallic phase so obtained presents a global stoichiometry of $Pt(SnBu_{2.7})_{1.4}/SiO_2$. When a PtSn−OM-type phase is activated in hydrogen at 773 K, it is transformed into a bimetallic $PtSn/SiO_2$ catalyst, denoted PtSn−BM (reaction 4).

Results of hydrogen and carbon monoxide chemisorption showed H(CO)/Pt values between 0.6 and 0.7 (Table 2), which indicate a high dispersion of the metallic phase. An important decrease in H(CO)/Pt values is observed for tin-modified catalysts. In this case, the bimetallic phase chemisorbs gas up to a ratio of approximately 0.20−0.25 H(CO)Pt, which might be ascribed to an homogeneous and specific deposition of tin over superficial platinum, without discarding the possibility that electronic modifications generated by tin may contribute to this effect. Previously published results of TEM measurements showed that the particle-size distribution of both mono- and bimetallic catalysts were very narrow, with a mean particle diameter around 2.0 nm for Pt/SiO_2 and with a slight increase in the mean for PtSn−BM on the order of 0.5 nm.[25] The variation in particle size is in agreement with the results obtained

TABLE 2: H_2/CO Chemisorption and XPS Results for PtSn−BM, PtSn−OM, and PtSn−OM* Systems

entry		1	6	7	13	14
catalyst		Pt/SiO_2	PtSn−OM	PtSn−OM*	PtSn−BM	PtSn−BM
H/Pt		0.64	nd	nd	0.21	0.20
CO/Pt		0.56	nd	nd	0.25	0.24
binding energy (BE)	Pt $4f_{7/2}$	71.6	70.8	70.6	70.9	70.6
	Sn(0) $3d_{5/2}$		484.3	484.6	485.0	484.6
	Sn(II, IV) $3d_{5/2}$		487.0		487.0	486.5
Sn(0)/[Sn(0) + Sn(II, IV)]			0.45	1.00	0.67	0.64

by other authors for $PtSn/\gamma$-Al_2O_3 catalysts prepared using an analogous methodology.[26] The authors also assigned the decrease in the quantity of chemisorbed hydrogen to the selective deposition of tin onto platinum.

Pt/SiO_2, PtSn−OM, PtSn−OM*, and PtSn−BM samples (entries 1, 6, 7, 13, and 14 in Table 1) were chosen for characterization by XPS and/or EXAFS. The PtSn−OM catalyst is a phase whose stoichiometry was determined as $Pt[SnBu_{1.8}]_{0.4}/SiO_2$; the PtSn−OM* catalyst consists of the phase having a stoichiometry of $PtSn_{0.4}/SiO_2$. The PtSn−BM catalysts present a stoichiometry of $PtSn_x/SiO_2$ ($x = 0.4$ or 0.7) and are obtained by activation in H_2 at 773 K of the corresponding PtSn−OM catalyst.

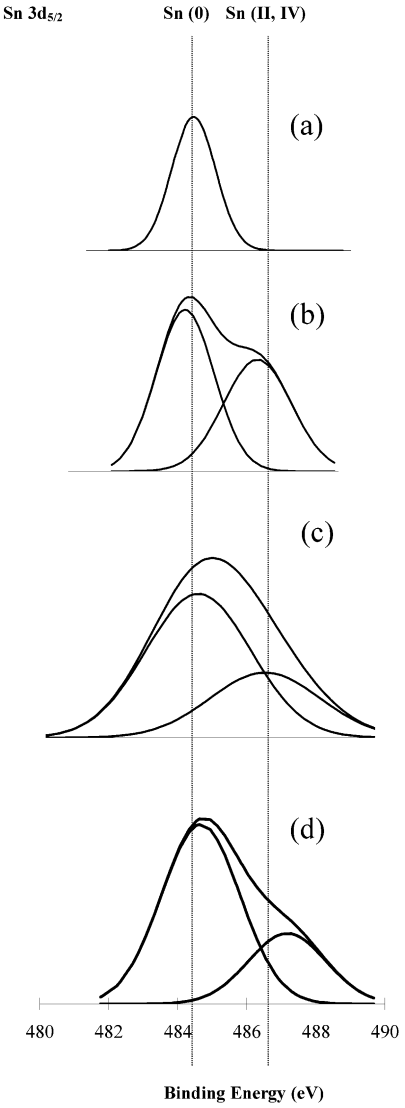

Figure 1. XPS spectra of Sn $3d_{5/2}$ level for (a) PtSn−OM* (entry 7), (b) PtSn−OM (entry 6), (c) PtSn−BM (entry 13), and (d) PtSn−BM (entry 14).

Table 2 shows XPS results giving the position of all of the main photoelectron peaks after referencing them to the C1s BE of 284.6 eV, and Figure 1 shows the XPS spectra of the Sn $3d_{5/2}$ level for the tin-modified catalysts. For all of the studied catalysts in the region corresponding to Pt $4f_{7/2}$ (around 71 eV), only one peak appears, indicating the complete reduction of platinum. In considering this peak, an interesting aspect arises: in the three systems modified by tin, a shift is observed in the BE toward lower values of approximately 0.7−1 eV with respect to Pt/SiO_2. In relation to PtSn−OM and PtSn−BM catalysts, two peaks are also observed around 485 and 487 eV, which could be assigned to metallic tin (Sn(0)) and ionic tin (Sn(II, IV)), respectively. For the PtSn−OM sample, Sn(0) and Sn(II, IV) are found in similar proportions, whereas for the PtSn−BM samples, approximately 70% is found as Sn(0) and the remaining part is found as Sn(II, IV). The PtSn−OM* sample presents different behavior in relation to the other tin-modified catalysts, showing only one peak in the region of Sn $3d_{5/2}$ at 484.6 eV, which indicates that all tin is found as Sn(0).

X-ray Absorption Spectroscopy. XANES data were obtained for Pt/SiO_2 and PtSn−BM catalysts in H_2 and in Ar after evacuation and for a Pt foil reference at the Pt L_2 and L_3 absorption edges.

The normalized $L_{2,3}$ XANES spectra of both samples in H_2 and of the Pt foil reference are compared in Figures 2 and 3. Neither the L_2 nor the L_3 absorption edge of the Pt/SiO_2 sample exhibits a substantial energy shift relative to that of the foil. Difference spectra were obtained by subtracting the Pt foil reference spectrum from that of the sample at each edge. The L_2 difference spectrum (Figure 2.a) contains a very weak negative peak near the edge and a strong positive peak 8 eV from the edge, whereas the L_3 difference spectrum (Figure 2b) contains a stronger negative feature after the edge and a similar positive peak at 8 eV. These results for reduced Pt/SiO_2 have already been reported in the literature.[22] Ramaker et al. have

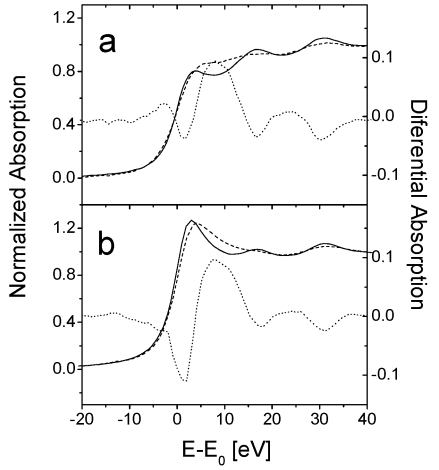

Figure 2. Comparison between the absorption L_2 (a) and L_3 (b) edges of Pt/SiO_2 (entry 1) in H_2 (dotted line) and bulk Pt (solid line). Dashed lines show the difference spectra.

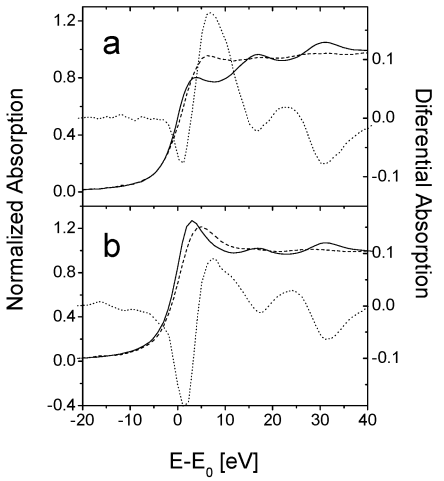

Figure 3. Comparison between the absorption L_2 (a) and L_3 (b) edges of PtSnBM (entry 14) in H_2 (dotted line) and bulk Pt (solid line). Dashed lines show the difference spectra.

proposed that these peaks at 8 eV can be attributed to the presence of chemisorbed hydrogen on Pt atoms.[27] Structure-related features are observed in each difference spectrum at 15−40 eV. The negative sense of these features indicates the presence in the spectrum of Pt foil but the absence in the spectra of the samples. The negative feature at 15 eV present in both L_2 and L_3 difference spectra resembles in position the maximum of the first oscillation beyond the L_3 white line of the Pt foil. Hence, this negative feature can be attributed to a reduction in the coordination number of Pt in going from the foil to the clusters.[28]

The normalized Pt $L_{2,3}$ spectra of the bimetallic catalyst in H_2 and a Pt foil reference are compared in Figure 3. The L_3 absorption edge of this sample exhibits a shift of 0.8 eV to higher energy related to the reference, but the L_2 edge has no energy shift and only a change in the edge shape. The L_2 difference spectrum (Figure 3a) shows a positive broad feature at 7 eV, but the L_3 difference spectrum (Figure 3b) shows a negative sharp peak near the edge and a positive peak at 7 eV. Structure-related features appear again in the 15−40 eV region. The negative feature at 15 eV found for the monometallic catalyst is also present and is attributed again to a reduction of the coordination number of Pt related to Pt foil.

It has been already shown that the adsorption of H_2 on Pt crystallites on different supports has important effects on its XANES spectra.[27,29,30] Figures 4 and 5 show the normalized $L_{2,3}$ XANES spectra of both samples in Ar. Differences between the reference and the catalyst near the edge are smaller than those obtained in H_2. The L_2 difference spectrum for the monometallic catalyst (Figure 4a) contains a very weak positive feature at 5 eV, but the L_3 difference spectrum (Figure 4b) contains a weak negative feature before the edge and a similar positive peak at 5 eV. As in the spectra obtained in the H_2 atmosphere, structure-related features are observed in each difference spectrum at 15−40 eV.

The normalized Pt $L_{2,3}$ spectra of the bimetallic catalyst and a Pt foil reference are compared in Figure 5. The L_3 absorption edge of this sample exhibits a shift of 0.6 eV to higher energy related to the reference, but the L_2 edge has no energy shift and only a change in the edge shape. This might indicate that interaction of Sn atoms with the $5d_{5/2}$ state differs from that of the $5d_{3/2}$ state of platinum. Difference spectra between the bimetallic catalyst and Pt foil reference are also shown in Figure 5. The L_2 difference spectrum (Figure 5a) shows a positive broad

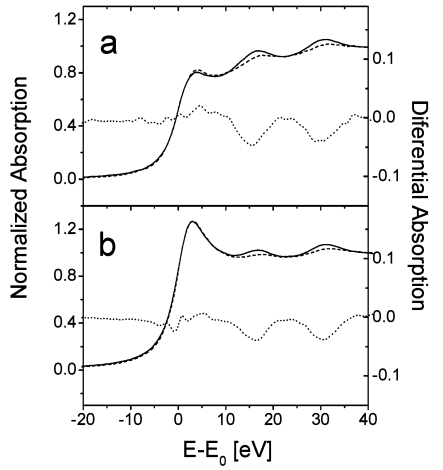

Figure 4. Comparison between the absorption L_2 (a) and L_3 (b) edges of Pt/SiO_2 (entry 1) in Ar (dotted line) and bulk Pt (solid line). Dashed lines show the difference spectra.

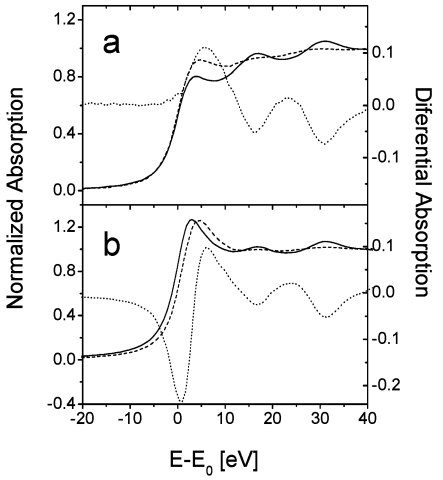

Figure 5. Comparison between the absorption L_2 (a) and L_3 (b) edges of PtSnBM (entry 14) in Ar (dotted line) and bulk Pt (solid line). Dashed lines show the difference spectra.

feature at 7 eV, but the L_3 difference spectrum (Figure 5b) shows a negative sharp peak near the edge and a positive peak at 7 eV. Structure-related features appear again in the 15−40 eV region.

Figures 6 and 7 show the k^3-weighted Fourier transforms of EXAFS L_3-edge spectra of the catalyst in H_2 and Ar atmospheres, also known as the radial distribution function. The solid line shows the amplitude and imaginary part of the Fourier transforms. Dashed lines show the amplitude and the imaginary part of the fitted EXAFS functions whose parameters are shown in Table 3.

Figure 6a shows the Fourier transform of the Pt/SiO_2 catalyst in H_2. Only one peak at 2.6 Å (without phase correction) is observed, suggesting that all Pt is in a reduced state, forming metallic particles. Figure 6b and c show Fourier transforms of PtSn−OM and PtSn−OM*, respectively. Both show a similar pattern with a broad contribution of scattering atoms between 1 and 3 Å, owing to at least two types of atoms. Figure 6d shows the Fourier transform of the bimetallic PtSn−BM catalyst. Two peaks at 2 and 2.6 Å (without phase corrections) are observed, possibly showing the existence of bimetallic particles in the catalyst.

Figure 7 shows the k^3-weighted Fourier transforms of EXAFS L_3-edge spectra of samples in Ar. Figure 7a shows the Fourier transform of the spectrum of Pt/SiO_2, and Figure 7b shows the

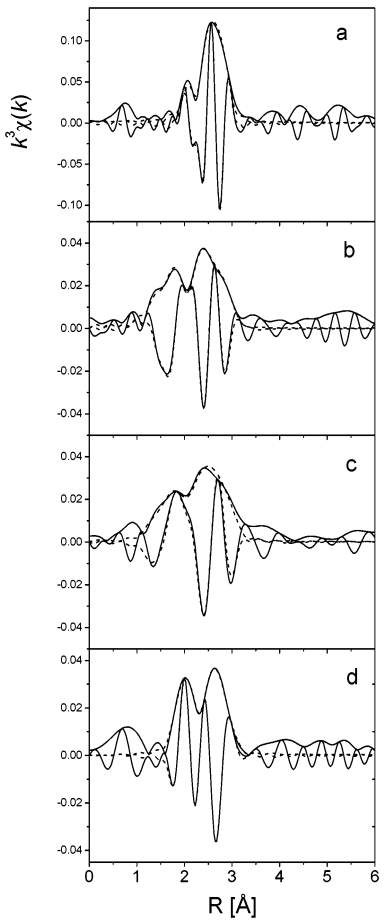

Figure 6. Fourier transforms of EXAFS data of samples in H_2: (a) Pt/SiO_2 (entry 1), (b) PtSnOM (entry 6), (c) PtSnOM* (entry 7), and (d) PtSnBM (entry 14). Solid lines show the amplitude and imaginary part of the Fourier transforms. Dashed lines show the corresponding Fourier transforms of the fitted functions.

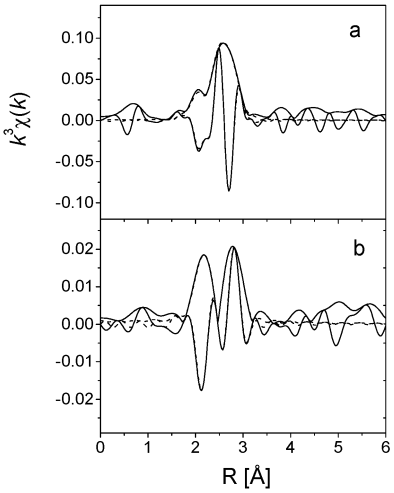

Figure 7. Fourier transforms of EXAFS data of samples in Ar. (a) Pt/SiO_2 (entry 1) and (b) PtSnBM (entry 14). Solid lines show the amplitude and imaginary part of the Fourier transforms. Dashed lines show the corresponding Fourier transforms of the fitted functions.

Fourier transform of the spectrum of bimetallic catalyst PtSn−BM. Both Fourier transforms are very similar to those found in the H_2 atmosphere for both catalysts. Only one peak at 2.6 Å is present in the Fourier transform corresponding to the monometallic catalyst. In the case of the bimetallic catalyst, two peaks are again present (one at 2.1 Å and the other at 2.7 Å).

TABLE 3: EXAFS Analysis[a]

entry	catalyst	pair	coordination number N	distance R (Å)	σ^2 (Å^{-2})	E_0 (eV)
1	Pt/SiO_2 [H_2]	Pt−Pt	8.3(1)	2.73(1)	0.0064(2)	6.2(3)
6	PtSn−OM	Pt−C	6(1)	1.98(5)	0.025(2)	4.5(3)
		Pt−Pt	6.7(6)	2.68(1)	0.011(1)	4.9(3)
7	PtSn−OM*	Pt−C	4.4(5)	2.0(1)	0.0084(5)	5.7(3)
		Pt−Pt	7.9(5)	2.67(2)	0.0096(3)	5.0(4)
14	PtSn−BM [H_2]	Pt−Sn	2.7(1)	2.68(1)	0.0055(1)	5.57(4)
		Pt−Pt	1.8(1)	2.71(2)	0.0032(8)	−1.82(8)
1	Pt/SiO_2 [Ar]	Pt−Pt	8.5(1)	2.71(1)	0.0081(1)	5.6(3)
14	PtSn−BM [Ar]	Pt−O	1.1(1)	1.99(1)	0.0039(2)	4.7(3)
		Pt−Sn	2.7(1)	2.65(1)	0.0092(4)	5.6(3)
		Pt−Pt	4.1(2)	2.71(1)	0.0074(3)	3.5(3)

[a] Bond distances, coordination numbers, Debye−Waller factors, and the parameter E_0.

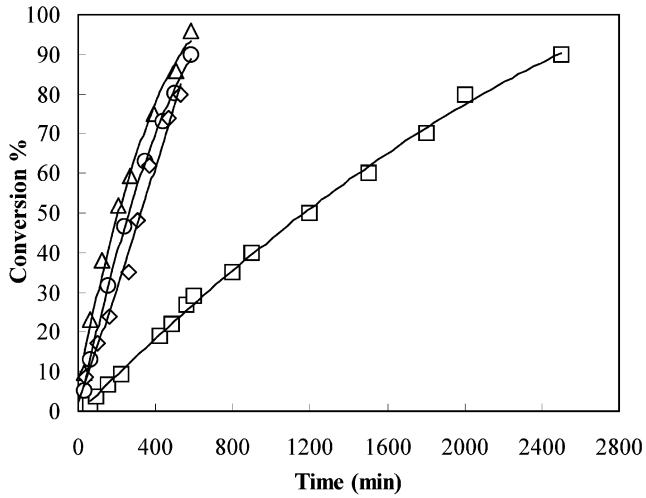

Figure 8. Conversion of cinnamaldehyde as a function of time for (□) Pt/SiO_2 (entry 1), (○) PtSn−BM (entry 13), (△) PtSn−OM (entry 6), and (◇) PtSn−OM* (entry 7). For experimental conditions, see the text.

To analyze these data quantitatively, the main peaks were isolated and fitted using standard procedures.[31] Different combination of shells were used to fit each spectrum. Theoretical standards were generated by the FEFF program.[32] In the fitting, the bond distances, coordination numbers, Debye−Waller factors, and E_0 parameter for each atomic pair were allowed to vary independently. The reduction factor S_0^2 was obtained from a Pt foil and was kept fixed for all samples. Results are shown in Table 3. The monometallic sample shows similar results in both atmospheres. In both cases, only a Pt−Pt shell was fitted, indicating that the Pt on these samples is in metallic form. The average coordination number of the Pt−Pt shell for these two samples is smaller than 12, which is the average coordination number for the Pt foil, indicating the small size of the crystals.

EXAFS spectra of PtSn−OM and PtSn−OM* were fitted using two shells—one Pt−C shell and one Pt−Pt shell (Table 3). Even the fits are in agreement with experimental data; other atoms could be present in the surroundings of some Pt atoms, though because of its small contributions a confident fit with more shells would not be possible. Some differences are found between the fitted parameters of each sample. The number of Pt first neighbors is smaller in the PtSn−OM sample, and the number of C neighbor atoms is larger. The average coordination number for Pt−Pt of both samples is smaller than that of the monometallic sample, indicating the isolation of Pt particles due to the presence of organotin fragments.

SCHEME 1: Reaction Pathways for the Hydrogenation of Cinnamaldehyde

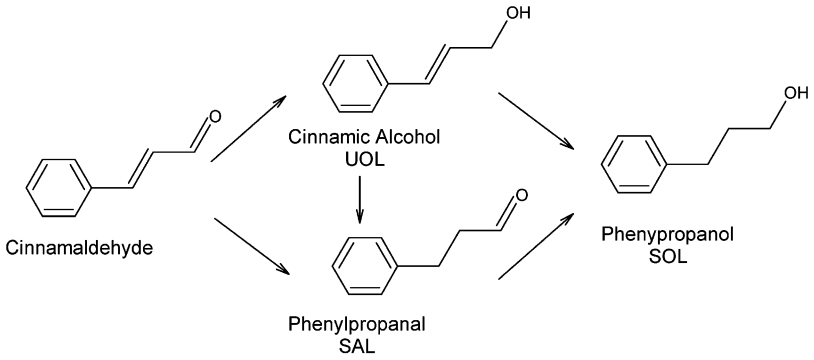

TABLE 4: Selectivity to SAL, UOL, and SOL at 10% Conversion for All of the Studied Catalysts[a]

entry	catalyst	S_{SAL} %	S_{UOL} %	S_{SOL} %
1	Pt/SiO_2	66.15	25.88	7.96
2	PtSn−OM*	37.55	62.45	
3	PtSn−OM*	31.70	68.30	
4	PtSn−OM*	29.10	68.00	2.79
5	PtSn−OM	23.00	73.80	3.20
6	PtSn−OM	20.58	77.80	1.62
7	PtSn−OM*	40.00	54.00	6.00
8	PtSn−OM	12.77	87.23	
9	PtSn−OM	10.56	89.44	
10	PtSn−BM	49.35	47.20	3.45
11	PtSn−BM	47.22	50.87	1.91
12	PtSn−BM	34.39	64.00	1.59
13	PtSn−BM	23.24	74.04	2.72
14	PtSn−BM	12.89	87.11	

[a] For experimental conditions, see the text.

The fits of PtSn−BM samples in both Ar and H_2 atmospheres show that there exist some differences in the formation of Pt structures. The sample in H_2 could be fitted using two shells corresponding to the first shells around Pt in a PtSn alloy.[33] The sample in Ar needed three shells—the same two first shells of Pt in PtSn−BM used in the fit of the sample in H_2 and an additional Pt−O shell. The other distinctive aspect of the fits is that the coordination number for the Pt−Pt distance is higher for the sample in Ar.

Hydrogenation of Cinnamaldehyde. In cinnamaldehyde, besides the double C═C bond and the C═O group, the benzene ring is susceptible to hydrogenation; hydrogenolysis reactions can also occur. Under the operating conditions used in this work, products that can be assigned to these reactions are not observed. The only products detected at quantifiable levels are, according to the pathways in Scheme 1, cinnamic alcohol (UOL), phenylpropanal (SAL), and phenylpropanol (SOL).

Figure 8 shows the conversion curves as a function of time for Pt/SiO_2, PtSn−BM, PtSn−OM, and PtSn−OM* systems (entries 1, 6, 7, and 13). The shape of these curves is compatible with a good level of stability of the active phases, and a reaction order near zero with respect to cinnamaldehyde is in a good agreement with results published in the literature on PtSn and RuSn.[34]

Table 4 shows the catalytic results of the cinnamaldehyde hydrogenation for these systems. In the case of the monometallic catalyst, the major product is the saturated aldehyde; S_{UOL} is maintained at less than 30%. The tin addition produces a noticeable change in the distribution of products, increasing S_{UOL} and decreasing S_{SAL}. As can be seen in Figure 9, S_{UOL} for tin-modified catalysts is much higher than for monometallic catalysts in the complete interval of conversions, according to the following sequence for S_{UOL}: PtSn−OM > PtSn−BM ≫ PtSn−OM* ≫ Pt/SiO_2. It is very interesting to observe the Sn effect on the reaction rate and on the selectivity to UOL. These results are presented in Figures 10 and 11 as a function of the Sn/Pt atomic ratio for the OM and BM series, respectively. For all of the tin concentrations analyzed, the hydrogenation rate suffers an increase with respect to that of the monometallic Pt/SiO_2 catalyst, reaching the maximum values for Sn/Pt between 0.2 and 0.4. Starting from Sn/Pt higher than 0.3, the S_{UOL} is markedly promoted by tin, reaching values between 80 and 90%. In all cases, the catalysts of the OM series show S_{UOL} values higher than those of the BM series.

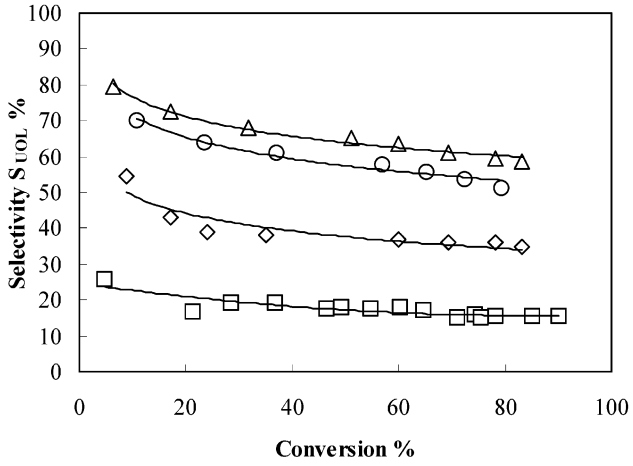

Figure 9. Cinnamaldehyde hydrogenation. Selectivity to UOL as a function of conversion for (□) Pt/SiO_2 (entry 1), (○) PtSn−BM (entry 13), (△) PtSn−OM (entry 6), and (◊) PtSn−OM* (entry 7). For experimental conditions, see the text.

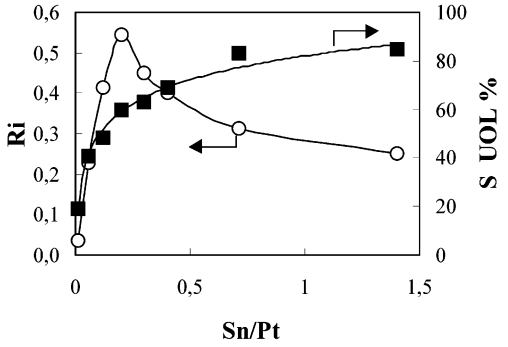

Figure 10. Hydrogenation of cinnamaldehyde for PtSnOM catalysts as a function of the Sn/Pt atomic ratio. (○) Formation rate (mmol s^{-1} g_{Pts}^{-1}) of UOL (estimated between conversion 0 and 10%) and (■) selectivities to UOL at 40% conversion. For experimental conditions, see the text.

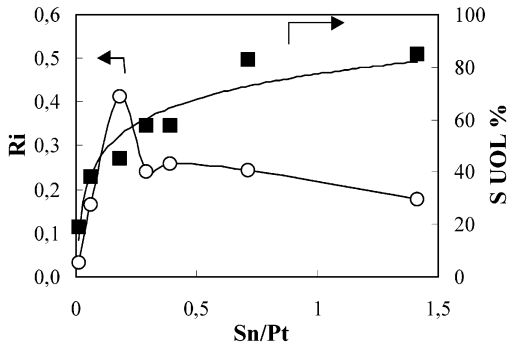

Figure 11. Hydrogenation of cinnamaldehyde for PtSnBM catalysts as a function of the Sn/Pt atomic ratio. (○) Formation rate (mmol s^{-1} g_{Pts}^{-1}) of UOL (estimated between conversion 0 and 10%) and (■) selectivities to UOL at 40% conversion. For experimental conditions, see the text.

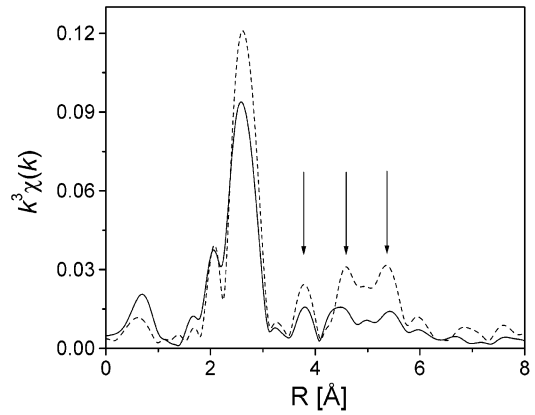

Figure 12. Comparison of the radial distribution functions of the Pt foil (dashed line) and the Pt/SiO_2 catalyst in Ar. Arrows show the positions of the second, third, and fourth coordination shells. The Pt foil Fourier amplitude was divided by 2 for scaling purposes

Discussion

EXAFS experiments of Pt/SiO_2 and tin-modified platinum catalysts demonstrate that the Sn addition has strong effects on Pt structures. This is clearly evident just from the comparison of the Fourier transforms of EXAFS spectra of both samples. The analysis of the parameters obtained from the fit of these spectra let us obtain important information on the structures present in each catalyst.

The monometallic catalyst shows a similar radial distribution function in both atmospheres, H_2 and Ar. In both samples, the presence of only one type of scatterer atom for Pt in their radial distribution functions is observed. They are perfectly fitted, proposing only a Pt−Pt shell. No evidence of a Pt−O shell is present, which would appear as a peak at a distance of 1.7 Å.[35] All Pt is in a reduced state forming metallic particles, in agreement with the XPS results shown in Table 2. Practically no difference is observed in the average coordination number fitted. Figure 12 shows a comparison between the Fourier transform of the spectra of Pt/SiO_2 in Ar and a Pt foil. The amplitude of the Pt foil Fourier transform has been divided by 2 in the figure so that spectra can be more easily compared. The arrows indicate the positions of higher Pt shells. It is clearly observed that second, third, and even fourth Pt shells are present in the catalyst, indicating that Pt crystallites have 3D fcc structures. The fitted average coordination numbers are lower than that of bulk Pt, indicating the small size of Pt particles. When small metal clusters are examined by EXAFS, the average coordination number is smaller than the one observed in the bulk because of the high proportion of surface atoms. This effect is dependent on the size and shape of the metallic cluster. The platinum particle size in Pt/SiO_2 after reduction may be estimated from coordination number *N* obtained for the Pt−Pt shell according to the method proposed in the literature,[36] assuming the spherical particle of the fcc package. From our results, the diameter of the metallic particles is estimated to be between 12 and 14 Å in both samples (approximately 500 atoms), which is compatible with a high level of dispersion as shown by H/Pt values in Table 2. The Pt−Pt distance fitted for these clusters is 2.73 Å for H_2 and 2.71 Å for Ar; for the bulk Pt, it is 2.77 Å. The Pt−Pt bond contraction that is found is consistent with previous results.[37] In effect, it has been reported that nearest-neighbor distances determined from EXAFS measurements of "bare" (i.e., without adsorbed gases) Pt clusters show contractions of approximately 0.07 Å (2.5%) relative to the bond length in bulk Pt. This shorter metal−metal bond distance is in agreement with the known general trend observed in metallic clusters. (See, for example, ref 38 for experimental evidence and ref 39 for theoretical predictions.)

PtSn−OM and PtSn−OM* samples show a more complicated radial distribution function. At least two different scatterer atoms must be present to obtain such a result. Considering the way the catalysts are prepared, we use Pt−C and a Pt−Pt shell to perform the fits. Before the reduction process, a solvent fraction remains adsorbed on the samples, so the appearance of C in the vicinity of Pt atoms is natural. We do not expect the appearance of oxygen because samples are not exposed to an oxidizing atmosphere and the initial state (the monometallic Pt/SiO_2 catalyst) does not present such kinds of interactions. Anyway, experimental evidence is not enough to discard the presence of the very low contents of other scatterers, which could be as nearest-neighbor atoms.

Results show that the coordination number for the Pt−Pt shell is smaller in both samples than that of the monometallic sample. The coordination numbers for the Pt−C shells are higher for PtSn−OM. This is an expected result because of the presence of PtSnBux in this sample. However, considering that the same starting material was used for both samples and that temperatures during preparation were kept below 423 K, no change in the size of Pt particles is expected. Because of this, the diminution of the Pt−Pt coordination number should be an artifact of the fitting caused by the presence of the Pt−C shells and the inhomogeneity of the structure.

The PtSn−BM catalyst has a similar radial distribution function in both atmospheres. However, some differences are observed from the fitted parameters. The existence of a Pt−Sn alloy is evident from the results. Two shells are enough to obtain a very good fit for the sample in H_2 consisting of Pt−Pt and Pt−Sn shells. When the H_2 is evacuated and the sample is kept in an inert atmosphere of Ar, a Pt−O shell appears, and an important increase in the coordination number of the Pt−Pt shell is observed. We will first analyze results in H_2 to explain this behavior.

It has been reported that PtSn and Pt_3Sn are the most abundant alloys in Pt−Sn bimetallic systems.[40] For this reason, we will consider these two alloys in our analysis. In Pt_3Sn, Pt atoms have 12 first-neighbor Pt atoms and 4 first-neighbor Sn atoms at a distance of 2.828 Å.[41] If the structure present in our catalyst was this type of alloy, then one would expect a ratio of Pt and Sn atoms in the first coordination of 3 to 1. This is clearly not the case from our fits (Table 3). Moreover, the distances are not equal for the two types of atoms as in the alloy. Thus, we would not expect our bimetallic particles to have the structure

of this alloy. In contrast, in the PtSn alloy, Pt has 2 Pt atoms at 2.72 Å and 6 Sn atoms at 2.73 Å. In this case, one would expect a Pt/Sn coordination ratio of 1 to 3. This is closer to the ratio found in our case (Table 3). However, the distances for each coordination shell are inverted. That is, Sn atoms are closer than Pt atoms in our sample, contrary to what happens in the alloy, though differences are small. This can be understood in terms of the coexistence of two different phases in the catalyst: a PtSn alloy and some unalloyed Pt particles. The unalloyed Pt phase would contribute to the Pt−Pt shell increasing both its coordination number and its distance. This would explain why the ratio between coordination numbers for the Pt−Pt and Pt−Sn shells is not 1 to 3 as expected for the PtSn alloy. In addition, Borgna et al. have shown that the presence of the peak at 2.15 Å found in the radial distribution function is not only a fingerprint for Pt−Sn interactions but also evidence of the existence of unalloyed Pt.[42]

When the bimetallic is sealed in Ar, some changes in the alloy structure are found. The most noticeable aspects are the appearance of a Pt−O shell and the increase in the Pt−Pt coordination number. Both of them are related. It has been shown for NiSn bimetallic catalysts that when they are exposed to an inert gas the metal with a lower sublimation point is segregated from the alloy.[43,44] In our case, Sn would be segregated from the PtSn alloy, increasing the size of the Pt particles and thus increasing the Pt−Pt average coordination number and making more important the interaction with the SiO_2 support, which could be the explanation of the Pt−O shell. These interactions may be present in the sample in H_2, but because of its small contribution to the total signal, it cannot be fitted confidently.

The coexistence of the PtSn alloy and an unalloyed metallic Pt phase can be confirmed by considering the number of Pt and Sn atoms in the catalyst. Thus, there are more Pt atoms than Sn atoms available to form the alloy (Sn(0)/Pt = 0.5 from XPS results presented in Table 2). Because the stoichiometry of the alloy is PtSn, the rest of the Pt atoms should be in a metallic state because no other type of scatterer is found in our EXAFS results, indicating that there are no other Pt phases present. Besides, XPS results indicate that platinum was completely reduced in this sample.

XANES data show that the addition of Sn has important effects on the electronic structure of Pt. This is not surprising because the EXAFS results show the existence of a PtSn alloy in the bimetallic sample. To quantify this effect, we estimated changes in the d band of Pt. Calculations of the number of holes in the d band of platinum clusters and bimetallic clusters were performed following a variation of the method proposed by Mansour et al.[15] Edges of samples and the Pt foil were aligned, and their differences were numerically integrated from −10 to 14 eV. The fractional change in the total number of unfilled states in the d band of the sample compared to the number in the platinum foil (f_d) was calculated using eq 1. The number of unfilled d states in the sample (h_{Ts}) was calculated from eq 2, using 1.6 as the number of unfilled 5d states in platinum.[45] Results are summarized in Table 5. It was found that the average platinum atoms in both the monometallic and the bimetallic samples in H_2 have fewer 5d electrons than bulk platinum atoms, with the number of holes in the PtSn−BM sample being higher than that in the Pt/SiO_2 sample. Because the chemisorption of hydrogen has an important effect on the electron properties of Pt particles,[27,30] we measured the same samples in Ar to separate the effect of the tin addition from the one produced by hydrogen. Results in Ar show that there is practically no change in the number of d holes for the monometallic catalyst, with the change observed previously being caused only by the H_2 adsorption. For the PtSn−BM catalyst in Ar, there is an increase in the number of d holes relative to the number in the Pt foil (Table 5), but this increase is smaller than that found in H_2.

TABLE 5: Intensity of Pt L_2 and L_3 X-ray Absorption Edges on Pt/SiO_2 and $PtSn/SiO_2$ in Ar and in H_2[a]

entry	sample	ΔA_2	ΔA_3	f_d	h_{Ts}
1	Pt/SiO_2 in Ar	−0.04	0.09	0.017	1.627
14	PtSn−BM in Ar	1.12	0.01	0.08	1.728
1	Pt/SiO_2 in H_2	0.62	0.46	0.116	1.785
14	PtSn−BM in H_2	1.66	0.30	0.17	1.872

[a] Their corresponding fractional change in the total number of unfilled states in the d band compared to the number in the platinum foil (f_d) and the number of unfilled d states in the samples (h_{Ts})

A 5d hole density on metal atoms covered with hydrogen higher than the electron density in the bulk metal has been published for Pt/γ-Al_2O_3,[46] Pt/H-LTL,[47] and Pt/SiO_2[15] catalysts, but no previous calculation for the bimetallic PtSn catalyst has been reported. However, Stagg et al.[48] found for $PtSn/ZrO_2$ catalysts that the L_3 white-line intensity was much lower than that for the Pt foil, which would indicate a lower number of d holes than in the Pt foil. The same result was found by Román-Martínez et al.[49] for PtSn/C catalysts. Nevertheless, they have not investigated the L_2 edge, so a conclusion on the number of d holes is not possible on the basis of only their results. Jeon et al.[50] showed that Pt atoms in a PtSn alloy have a 5d electron population smaller than that of the atoms in metallic Pt. This is consistent with our results, considering the appearance of a PtSn alloy in the bimetallic catalyst. Rodríguez et al. have made ab initio self-consistent-field calculations that predict a small shift of s and p electrons from Sn toward Pt in 2D systems.[51] The formation of a Pt−Sn bond leads to an increase in the Pt (6s, 6p) electron population and a decrease in the Pt (5d) population, as shown in our results. This phenomenon is equivalent to a d → s, p rehybridization that moves electrons around Pt into the Pt−Sn bond. Our results would show that a similar rehybridization process could also be taking place in PtSn 3D small nanoclusters. In this context, the binding energy shifting (of about 1 eV) to higher values at the Pt 4f level observed in XPS results for bimetallic samples with respect to those for the monometallic samples would originate in the electronic transfer from the Pt 4f level to the Pt−Sn bond.

Results obtained from the characterization of Pt/SiO_2 phases and from the systems modified by Sn permit us to interpret the catalytic behavior of these phases in the selective hydrogenation of cinnamaldehyde. As previously mentioned, in all catalysts studied, the Pt is found to be completely reduced. The modified systems with Sn named PtSn−OM and PtSn−OM* (used in an H_2 atmosphere at temperatures below 423 K) do not present PtSn alloys. In the case of PtSn−OM*, which does not present Bu groups anchored on the surface or Sn(II, IV) (according to XPS results), Pt atoms would be isolated by Sn(0) adatoms "decorating" the metallic surface. In the PtSn−OM catalyst, Bu groups remain grafted on the surface, with Sn in the form of Sn(0) and Sn(II, IV) in similar proportions. The image of the active phase would be represented by Pt atoms isolated by PtSnBux islets, as represented in Scheme 2a. In bimetallic systems PtSn−BM, it is possible to observe that a part of the Pt is alloyed with the metallic Sn (PtSn, according to EXAFS results) and that the other part of the Pt is alloyed with metallic Pt atoms isolated from such an alloy. There also exists a Sn percentage of ionic nature (20−30%), probably placed in the

SCHEME 2: Representations of Catalytic Surfaces for (a) PtSnOM and PtSnOM* and (b) PtSnBM

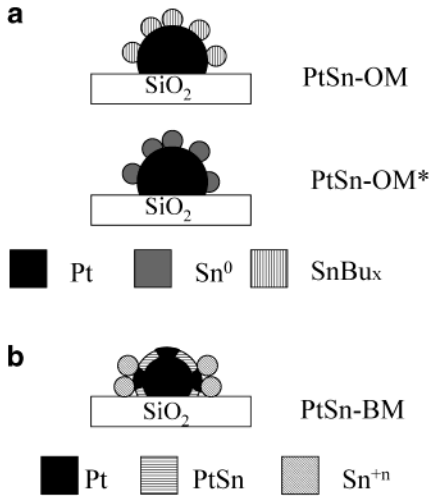

metal−support interface. The image of the catalytic surface for PtSn−BM can be represented by Scheme 2b.

In the hydrogenation of cinnamaldehyde, as observed in Figure 8 and in Table 4, the hydrogenation rate of the C═O group leading to UOL formation shows a noticeable increase in catalysts modified with tin with respect to Pt/SiO_2. The effect of site isolation generated by tin favors the presence of species leading to UOL, mainly of types η^1-(O) and η^2-(C,O), according to the classical scheme of adsorption proposed in the literature for α,β unsaturates aldehydes,[52] which is clearly favorable to the selectivity to UOL. However, the increase in the reaction rate seems rather controversial, taking into account the diminution in the quantity of chemisorbed hydrogen, at least when comparing PtSn−BM and Pt/SiO_2. This indicates that the chemisorbed hydrogen is enough, even in tin-modified catalysts, and that the chemisorption of hydrogen is not the rate-controlling step. The increase in the reaction rate has to be explained by a modification in the electronic nature of the active site, which agrees with our XANES results of an electronic transfer from Pt to the PtSn bond. In this same sense, recently published results regarding crotonaldehyde hydrogenation with SnPt(111) and Pt-(111) model catalysts showed an increase in the hydrogenation rate of a platinum−tin alloy with respect to platinum, which is explained by means of a reduction in the density of states at E_F. This is in agreement with scanning tunneling microscopy studies that give direct evidence of the mentioned electronic transfer. A lower activation energy for this reaction using a SnPt alloy with respect to Pt is also reported.[53,54]

Besides the existence of "Lewis acid sites", the presence of ionic tin promotes a better polarization of the C═O group, favoring the H_2 attack on it and, in this way, leading to a higher hydrogenation rate and higher selectivity for the unsaturated alcohol. Thus, the presence of ionic tin seems to have a positive effect on the increase in the UOL formation rate for the PtSn−OM and PtSn−BM systems compared to that for PtSn−OM*, in which ionic tin is not detected.

EXAFS results also contribute to extract some important conclusions with regard to the structure of the active phase. Taking into account that Sn(0) does not possess intrinsically hydrogenating properties, it seems reasonable to accept that PtSn alloys are not active in hydrogenation reactions and participate only in the isolation of the electronically modified Pt atoms. η^2-type adsorption is favored in PtSn−OM systems, which present Pt(0) atoms interacting with Sn(II, IV). This could explain the higher yields of UOL reached in these catalysts. In PtSn−BM catalysts, the presence of Pt(0) and Sn(II, IV) has also been determined, but in this case the interaction would be less efficient than for the PtSn−OM catalystprobably because of the location of the ionic tin.

Conclusions

Well-defined silica-supported Pt and PtSn catalysts were prepared by surface organometallic reactions and were characterized by XPS and XAFS techniques and the catalytic hydrogenation of cinnamaldehyde. The main conclusions can be summarized as follows:

XPS results show that in PtSn−OM* (not having Bu groups anchored on the surface) tin is present as Sn(0) adatoms "decorating" the metallic surface, isolating Pt atoms; in the PtSn−OM catalyst (Bu groups remain grafted on the surface), tin is found in the form of Sn(0) and Sn(II, IV) in similar proportions. EXAFS experiments do not evidence the existence of PtSn alloys in any of these systems.

In bimetallic systems PtSn−BM, it is possible to observe by XPS that tin is found in the form of Sn(0) and Sn(II, IV). EXAFS experiments, in this case, allow us to demonstrate the existence of a PtSn alloy diluting metallic Pt atoms.

A d → s, p rehybridization process could be taking place in PtSn 3D small nanoclusters, leading to an increase in the number of Pt 5d holes measured by Pt $L_{2,3}$ XANES.

In tin-modified systems, especially PtSn−OM and PtSn−BM where a fraction of ionic tin is present, the activation of the C═O group of the cinnamaldehyde is favored, increasing the selectivity to UOL.

Acknowledgment. This work has been sponsored by the Consejo Nacional de Investigaciones Científicas y Técnicas (CONICET, Argentina), the Agencia Nacional de Promoción Científica y Técnica (PICT no. 14-04378, Argentina), the Fundación Antorchas (Argentina), and the LNLS (Brazil) under project XAS 802/01.

References and Notes

(1) Jacobson, R. L.; Kludsdahl, M. E.; McCoy, C. S.; Davis, R. W. *Proc. − Am. Pet. Inst., Div. Refin.* **1969**, *49*, 504.
(2) Sinfelt, J. *Bimetallic Catalysts, Discovery, Concepts and Applications*; Wiley: New York, 1983.
(3) Santori, G.; Casella, M.; Ferretti, O. *J. Mol. Catal. A: Chem.* **2002**, *186*, 223.
(4) Siri, G. J.; Casella, M. L.; Santori, G. F.; Ferretti, O. A. *Ind. Eng. Chem. Res.* **1997**, *36*, 4821.
(5) Nichio, N.; Casella, M.; Santori, G.; Ponzi, E.; Ferretti, O. *Catal. Today* **2000**, *62*, 231.
(6) Rodríguez, J. A.; Goodman, D. W. *Science* **1992**, *257*, 897.
(7) Chojnacki, T. P.; Schmidt, L. D. *J. Catal.* **1991**, *129*, 473.
(8) Hansen, T. W.; Wagner, J. B.; Hansen, P. L.; Dahl, S.; Topsoe, H.; Jacobsen, C. J. H. *Science* **2001**, *294*, 1508.
(9) Prestvik, R.; Totdal, B.; Lyman, C. E.; Holmen, A. *J. Catal.* **1998**, *176*, 246.
(10) Lakis, R. E.; Lyman, C. E.; Stenger, H. G. *J. Catal.* **1995**, *154*, 261.
(11) Coloma, F.; Sepúlveda-Escribano, A.; Garcia Fierro, J. L.; Rodriguez-Reynoso, F. *Appl. Catal., A* **1996**, *136*, 231.
(12) Bazin, D. *Top. Catal.* **2002**, *18*, 79.
(13) Alexeev, O.; Gates, B. C. *Top. Catal.* **2000**, *10*, 273.
(14) Marcus, M. In *EXAFS Spectroscopy: Techniques and Applications*; Teo, B. K., Joy, D. C., Eds.; Plenum Press: New York, 1981; p 181.
(15) Mansour, A. N.; Cook, J. W.; Sayers, D. E. *J. Phys. Chem.* **1984**, *88*, 2330.
(16) Cook, J. W., Jr.; Sayers, D. E. *J. Appl. Phys.* **1981**, *52*, 5024.
(17) van Zon, J. B. A. D.; Koningsberger, D. C.; van't Blik, H. F. J.; Sayers, D. E. *J. Chem. Phys.* **1985**, *12*, 5742.
(18) Lee, P. A.; Citrin, P. H.; Eisenberger, P.; Kincaid, B. M. *Rev. Mod. Phys.* **1981**, *53*, 769.

(19) Lytle, F. W.; Wei, P. S. P.; Greegor, R. B.; Via, G. H.; Sinfelt, J. H. *J. Chem. Phys.* **1979**, *70*, 4849.
(20) Lytle, F. W. *J. Catal*. **1976**, *43*, 376.
(21) Meitzner, G.; Via, G. H.; Lytle, F. W.; Sinfelt, J. H. *J. Phys. Chem*. **1992**, *96*, 4960.
(22) Reifsnyder, S. N.; Otten, M. M.; Sayers, D. E.; Lamb, H. H. *J. Phys. Chem. B* **1997**, *101*, 4972.
(23) Brown, M.; Peierls, R. E.; Stern, E. A. *Phys. Rev. B* **1977**, *15*, 738.
(24) McMaster, W. H.; Kerr Del Grande, N.; Hubell, J. H. *Compilation of X-ray Cross Sections*; National Technical Information Service: Springfield, VA.
(25) Santori, G. F.; Casella, M. L.; Siri, G. J.; Adúriz, H. R.; Ferretti, O. A. *Appl. Catal. A: Gen.* **2000**, *197*, 141.
(26) Merlen, E.; Beccat, P.; Bertolini, G. R.; Delichère, P.; Zanier, N.; Didillon, B. *J. Catal.* **1996**, *159*, 178.
(27) Ramaker, D. E.; Mojet, B. L.; Garriga Oostenbrink, M. T.; Miller, J. T.; Koningsberger, D. C. *Phys. Chem. Chem. Phys*. **1999**, *1*, 2293.
(28) Samant, M. G.; Boudart, M. *J. Phys. Chem.* **1991**, *95*, 4070.
(29) Ankudinov, A. L.; Rehr, J. J.; Low, J.; Bare, S. R. *Phys. Rev. Lett*. **2001**, *86*, 1642.
(30) Asakura, K.; Kubota, T.; Chun, W.; Iwaqsawa, Y.; Otan, K.; Fujikawa, T. *J. Synchrotron Radiat*. **1999**, *6*, 439.
(31) Koningsberger, D. C.; Mojet, B. L.; van Dorssen, G. E.; Ramaker, D. E. *Top. Catal*. **2000**, *10*, 143.
(32) Zabinsky, S. I.; Rehr, J. J.; Ankudinov, A.; Albers, R. C.; Eller, M. J. *Phys. Rev. B* **1995**, *52*, 2995.
(33) Harris, I. R.; Norman, M.; Bryant, A. W. *J. Less-Common Met.* **1968**, *16*, 427.
(34) Tronconi, E.; Crisafully, L.; Galvagno, S.; Donato, A.; Neri, G.; Pietropaolo, R. *Ind. Eng. Chem. Res.* **1990**, *29*, 1766.
(35) Gutierrez, L. B.; Ramallo-López, J. M.; Irusta, S.; Miró, E. E.; Requejo, F. G. *J. Phys. Chem. B* **2001**, *105*, 9514.
(36) Greegor, R. B.; Lytle, F. W. *J. Catal*. **1980**, *63*, 476.
(37) Khodakov, A.; Barbouth, N.; Oudar, J.; Villain, F.; Bazin, D.; Dexpert, H.; Schulz, P. *J. Phys. Chem*. **1997**, *101*, 776.
(38) Klimenkov, M.; Nepijko, S.; Kuhlenbeck, H.; Bäumer, M.; Schlögl, R.; Freund, H. J. *Surf. Sci*. **1997**, *391*, 27.
(39) Ankudinov, A. L.; Rehr, J. J.; Low, J. J.; Bare, S. *J. Chem. Phys.* **2002**, *116*, 1911.
(40) Meitzner, G.; Via, G. H.; Lytle, F. W.; Fung, S. C.; Sinfelt, J. H. *J. Phys. Chem*. **1988**, *92*, 2925.
(41) Ellner, M. *J. Less-Common Met.* **1981**, *78*, 21.
(42) Borgna, A.; Stagg, S. M.; Resasco, D. E. *J. Phys. Chem. B* **1998**, *102*, 5077.
(43) Ferretti, O. A.; Bettega de Pauli, L. C.; Candy, J. P.; Mabillon, G.; Bournonville, J. P. *Stud. Surf. Sci. Catal*. **1987**, *31*, 713.
(44) Ferretti, O. A.; Casella, M. L. *Lat. Appl. Res.* **1995**, *25*, 125.
(45) Ankudinov, A. L.; Nesvizhskii, A. I.; Rehr, J. *J. Synchrotron Radiat.* **2001**, *8*, 92.
(46) Vaarkamp, M. Pd.D. Thesis, Eindhoven University of Technology, Eindhoven, The Netherlands, 1993.
(47) Vaarkamp, M.; Mojet, B. L.; Kappers, M. J.; Miller, J. T.; Koningsberger, D. C. *J. Phys. Chem.* **1995**, *99*, 16067.
(48) Stagg, S. M.; Romeo, E.; Padro, C.; Resasco, D. E. *J. Catal*. **1998**, *178*, 137.
(49) Román-Martínez, M. C.; Cazorla-Amorós, D.; Yamashita, H.; de Miguel, S.; Scelza, O. A. *Langmuir* **2000**, *16*, 1123.
(50) Jeon, Y.; Chen, J.; Croft, M. *Phys. Rev. B* **1994**, *50*, 6555.
(51) Rodriguez, J. A.; Chaturvedi, S.; Jirsak, T.; Hrbek, J. *J. Chem. Phys.* **1998**, *109*, 4052.
(52) Claus P. *Top. Catal*. **1998**, *5*, 51.
(53) Batzill, M.; Beck, D. E.; Koel, B. E. *Surf. Sci*. **2000**, *466*, L821.
(54) Jerdev, D. I.; Olivas, A.; Koel, B. E. *J. Catal.* **2002**, *205*, 278.